Intramolecularly resolved Kondo resonance of high-spin Fe(II)-porphyrin adsorbed on Au(111)

Weihua Wang,[1] Rui Pang,[2] Guowen Kuang,[1] Xingqiang Shi,[2] Xuesong Shang,[3] Pei Nian Liu,[3] and Nian Lin[1,*]

[1]*Department of Physics, The Hong Kong University of Science and Technology, Hong Kong, China*

[2]*South University of Science and Technology of China, Shenzhen, China*

[3]*Shanghai Key Laboratory of Functional Materials Chemistry and Institute of Fine Chemicals, East China University of Science and Technology, Meilong Road 130, Shanghai, China*

(Received 17 June 2014; revised manuscript received 27 October 2014; published 30 January 2015)

Using cryogenic scanning tunneling microscopy, we measured the electronic states and Kondo resonance of single Fe(II)-porphyrin molecules adsorbed on a Au(111) surface with intramolecular resolution. We found that the Fe(II) ion introduces a spin-polarized molecular state near the Fermi level. Tunneling spectroscopy revealed that this state gives rise to Kondo resonance exhibiting characteristics different from those of the Fe(II) spin state. Spin-polarized density functional theory calculations revealed that the molecule was weakly adsorbed on the surface, yet still switches its spin configuration from $S = 1$ to 2. The spin switching was found to be driven by three effects: a structural distortion of the macrocyclic ring from planar to saddle shaped, a weak chemical bonding between the Fe and the Au surface atom underneath, and weakened Fe-N bonds due to Au(111)-molecule charge transfer.

DOI: 10.1103/PhysRevB.91.045440 PACS number(s): 71.15.Mb, 68.37.Ef, 72.15.Qm, 75.30.Wx

I. INTRODUCTION

Ferrous porphyrins Fe(II)P have attracted intensive attention because of their potential technological applications and their structural similarity to chlorophyll and hemoglobin [1]. In gas phase, Fe(II) in FeP or Fe-phthalocyanine (FePc) is at an intermediate spin state of $S = 1$ [1–4]. The spin state of the ferrous porphyrins can be switched under changes of external environment such as temperature, pressure, light, and external ligands [4]. An alternative approach to achieving spin switching is to adsorb the molecule on a substrate. The underlying mechanisms include chemical interaction between Fe ion and substrate, by which the substrate forms a chemical bond with the Fe ion [5,6] and charge transfer [7,8]. Attachment of an axial ligand at Fe may also induce spin switching [9,10]. Recently, Bhandary *et al.* predicted that a strain-induced change of the spin state from $S = 1$ to 2 takes place in FeP when the molecule is adsorbed at a divacancy site in graphene [11,12]. The effect relies on a strong binding between the FeP and the substrate through the defect site. Here, we report on a different but simple way of realizing spin switching in FeP : to adsorb the molecule on a flat Au(111) surface. We demonstrate that although the FeP molecule does not form a strong chemical bond with the substrate and the Fe ion preserves its $3d^6$ configuration in the adsorbed molecule, the Fe(II) spin state still switches from $S = 1$ to 2. We found that the spin switching was driven cooperatively by multiple mechanisms, including (1) deformation of the macrocyclic ring, (2) Fe − Au(111) interaction, and (3) weakened Fe-N bonds, when the molecule is adsorbed on the surface.

Experimentally, the spin states of surface-adsorbed FeP and FePc have been probed by spin-polarized scanning tunneling spectroscopy (SP-STS) [13,14] and x-ray magnetic circular dichroism [15–20]. Kondo effect, an effect associated with spin flipping by screening electrons, has been used to probe the spin state of the surface-adsorbed FePc molecules [21–25]. Herein we use STS to probe the intramolecular spatial distribution of the Kondo resonance of FeP molecules synthesized by on-surface Fe metalation of free-base porphyrin on Au(111). We found that the Kondo resonance at the central Fe ion and the macrocyclic ring exhibit different Kondo temperatures and different Kondo line-shape factors. Spin-polarized density functional theory (SP-DFT) calculations revealed that the Kondo resonance extending to the macrocyclic ring originates from spin-split coupling between Fe and porphyrin macrocyclic ring, which creates a spin-polarized molecular state lying near the Fermi level. This state is a hybridized state of the highest occupied molecular orbital (HOMO) of the free-base porphyrin with a Fe $3d$ orbital. Moreover, the theory concluded that Fe(II) is at a high-spin state and the intramolecularly resolved spatial distribution of the Kondo resonance corroborated this picture.

II. EXPERIMENTAL AND THEORETICAL METHODS

The experiments were performed in an ultrahigh vacuum scanning tunneling microscope system (Omicron Nanotechnology). A single-crystalline Au(111) surface was cleaned by sputtering and annealing cycles. 5,15-bis-(4-bromophenyl)-10,20-diphenyl porphyrin (H_2TPP) molecules were deposited using an organic molecular evaporator on the Au(111) surface which was held at room temperature. Fe atoms were deposited using an *e*-beam evaporator on the sample to metalate the free-base H_2TPP. STM measurements were conducted at 4.9 K. A lock-in amplifier was used to acquire tunneling spectra. The modulation frequency was set at 1.5 kHz and the modulation voltage was set at 2 mV (20 mV) for acquiring Kondo (molecular states) spectra.

DFT calculations were performed on an Au(111)-(8×8) surface with three atomic layers in the slab model. Structural optimizations adopted gamma-point-only K sampling. While for electronic-structure simulations, including projected density of states (PDOS) curves and constant PDOS contour maps, $4 \times 4 \times 1$ K−point sampling and a Gaussian broadening of 0.02 eV were used. Both PBE [26] and an optimized version

*phnlin@ust.hk

of van der Waals (vdW) density functional [27] computations were performed. With vdW interaction, the H_2TPP adsorption height is 3.82 Å, while without vdW interaction the height is 5.93 Å which is far too large. Thus, the vdW functional gave more accurate adsorption height and the corresponding results were used. For FeTPP, these two functionals gave similar adsorption heights; and, in convenience to make comparing with similar systems in literature [28], the spin-polarized PBE results were present. The Hubbard U term was added to describe the transition-metal ion [29]. An effective $U, U - J = 6.0$ eV was obtained via artificial matching theoretical PDOSs to the experimental tunneling spectra (dI/dV), which was confirmed by the linear-response theory [30], giving an effective $U = 5.6$ eV. U values in the range of 3–6 eV by matching results in literatures and from computational consideration were used in gas-phase molecule calculations [31,32]. The main computations were carried out with VASP package [33,34]. The plane-wave cutoff energy is 400 eV. The Hubbard U was evaluated with Quantum Espresso [35].

III. RESULTS AND DISCUSSION

After thermal annealing at 100°C, FeTPP molecules were synthesized through on-surface metalation of H_2TPP molecules with Fe [36–38]. The FeTPP molecules either formed close-packed islands, as shown in Fig. 1(a), or were adsorbed on the surface as single molecules. Note that the structural and electronic characteristics of FeTPP are independent of the molecular organization. At a bias voltage of −1.0 V, the molecules show C_{2v} symmetry with a central maximum sandwiched between two shoulder features. We refer to the high-symmetric axis that passes through the central maximum and the two shoulders as the main axis as indicated by the dashed line in Fig. 1(a). Figure 1(b) shows site-specific tunneling spectra (dI/dV) measured at three locations along the main axis of a FeTPP molecule as marked by blue, red, and black dots in Fig. 1(a). The dI/dV spectrum from the site at the center (the black curve) shows a shoulder at −1.1 V, a dip at the Fermi level, a steplike feature at 0.2 V, and a peak at 1.4 V. The dI/dV spectra from the sites at the two sides show an asymmetric peak at −1.1 V, a salient peak at 1.4 V, and a sharp peak at 0.2 V. Figures 1(c)–1(e) show energy-resolved STS images of an isolated FeTPP molecule acquired at the three dI/dV peak energies, namely, −1.1, 0.2, and 1.4 V. The −1.1- and 0.2-V STS images are nearly identical, showing two triangular-shaped protrusions at the two opposite pyrrole rings along the main axis and a dim dot at each of the four corners. The 1.4-V STS image shows a four-leaf clover pattern with two nodal planes along and perpendicular to the main axis. All three STS images display C_{2v} symmetry.

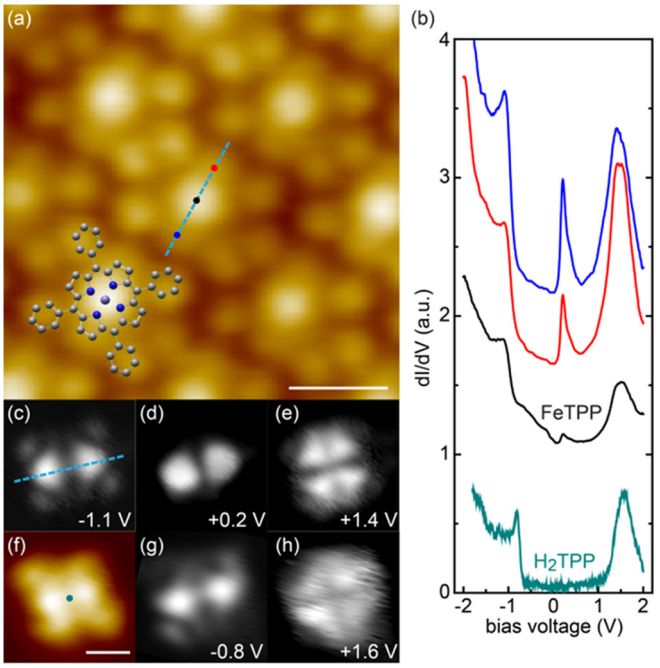

FIG. 1. (Color online) (a) STM topograph (−1.0 V, 0.3 nA) of on-surface-synthesized FeTPP molecules in a close-packed island. The dashed line indicates the main axis. A structural model is overlaid on one of the molecules. (b) Site-specific dI/dV spectra measured at the points marked in (a) following the same color coding, and at the center of a H_2TPP in (f). The spectra are shifted vertically for clarity. (c)–(e) STS images of a single FeTPP molecule at the indicated bias voltages. (f)–(h) STM topograph (−1.0 V, 0.3 nA) and STS images at the indicated bias voltages of a single H_2TPP molecule. The scale bars are 1 nm and (c)–(h) are in the same scale.

For comparison, we present the STM topograph, dI/dV spectrum, and STS images of a free-base H_2TPP molecule. In the STM topograph [Fig. 1(f)], the molecule center is not a protrusion but a depression, corroborating an unmetalated macrocyclic core. A dI/dV spectrum measured at the molecular center is shown in Fig. 1(b) bottom. It has two peaks at −0.8 and 1.6 V, corresponding to the HOMO and the lowest unoccupied molecule orbital (LUMO), respectively (see later discussion). The spectra acquired (not shown) at the two sides show similar features to that acquired at the center. The STS images acquired at −0.8 V [Fig. 1(g)] and 1.6 V [Fig. 1(h)] are comparable to the −1.1- and 1.4−V STS images of FeTPP, implying that the latter two states can be traced to the former two states, respectively. Fe metalation slightly down-shifts the HOMO (by 0.3 V) and LUMO (by 0.2 V) of H_2TPP. Note that around the Fermi level there are two new features emerged at FeTPP in contrast to H_2TPP: a peak at 0.2 V and a dip at the Fermi level. We attribute these new features to the Fe. Interestingly, this 0.2-V state is not localized at the central Fe but instead extends to the two pyrrole rings along the main axis, which resembles the shape of H_2TPP HOMO [38].

The dip feature at the Fermi level can be attributed to the Kondo effect arising from the interaction between the spin state of the Fe center in FeTPP and the screening electrons [21–25]. Our measurements show that the Kondo resonance of FeTPP is independent of the molecular adsorption site or the supramolecule assembly structure, which is in contrast to previous studies of FePc or CoTPP on Au(111) [23,39]. To resolve intramolecular Kondo features, we measured tunneling spectra along the red (main axis) and blue axes in Fig. 2(a). The spatially resolved spectra are plotted in Figs. 2(b) and 2(c). The spectra can be fitted by a Fano function [40] $\frac{dI}{dV} = A\frac{[q+(x-x_0)/\Gamma]^2}{1+[(x-x_0)/\Gamma]^2} + y_0$, in which A is the amplitude of the Kondo resonance, q the line-shape factor, x_0 the energy shift of resonance center from the Fermi level,

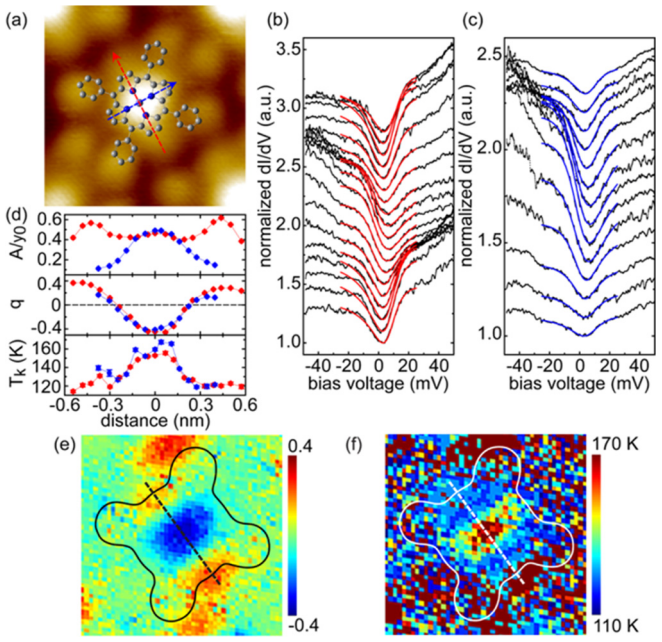

FIG. 2. (Color online) (a)–(c) Spatial evolution of normalized Kondo resonance in a FeTPP molecule. Spectra in (b) and (c) are measured along the red (main axis) and blue dashed lines in (a), respectively. The Fano fitting is shown by red and blue curves. (d) Spatially resolved normalized magnitude A/y_0, line-shape factor q, and Kondo temperature T_K derived from the Fano fitting of the spectra in (b) and (c) following the same color coding. (e), (f) 2D q and T_K maps ($2.0 \times 2.0\,\mathrm{nm}^2$).

y_0 the background dI/dV signal, and $\Gamma = k_B T_K$ the width of the resonance, where k_B is the Boltzmann constant and T_K is the Kondo temperature. The spatial evolution of the normalized amplitude A/y_0 is plotted in the top panel of Fig. 2(d). Generally speaking, amplitude of Kondo resonance depends on the tip lateral position offset from the scattering center (magnetic impurity or the spin-polarized states in our case) and the spin density underneath the tip [28,41]. In Fig. 2, the amplitude variation occurs within a molecule, so the effects from tip lateral position offset can be ignored. We attribute the spatial variation of Kondo resonance amplitudes to the spatial distribution of spin states within the molecule. Along the red (main) axis, besides a central maximum there are two maxima at the pyrrole rings with even higher intensity than the central maximum. Apparently, the two side maxima are not contributed by the central Fe ion, but by the spin-polarized molecular states at the pyrrole rings [39].

The line-shape factor q and the Kondo temperature T_k, plotted in the middle and bottom panels of Fig. 2(d), respectively, also display intramolecular spatial variation. Specifically, q takes a value of ~ -0.4 at the molecule center, i.e., at the Fe ion, whereas at the two pyrrole rings along the main axis q takes a value of $\sim +0.4$. The absolute value of q reflects the competition of two tunneling channels of tunneling to the spin state and to the continuous state. The sign of q is determined by the interference phase between the two tunneling channels [42,43]. Sign inversion of q may happen when the tip is laterally off a single magnetic impurity or when the tip is positioned at different magnetic centers. For a single magnetic impurity on Au(111), the line-shape factor changes its sign when the tip is $\sim$1.6 nm laterally off the impurity owing to the surface band structure [44,45]. The observed line-shape variation within single FeTPP molecules is about a quarter of this distance. Thus, we rule out the surface band contribution but rather attribute the sign inversion of q to different scattering centers within a molecule. The sign inversion of q at the Fe center versus that at the pyrrole rings suggests the spin states at the Fe ion and those at the pyrrole rings are of different characteristics. The Kondo temperature falls in the range of 150–170 K at the molecule center and in the range of 120–130 K at the pyrrole rings. This contrast may reflect that (1) the coupling between the itinerary electrons and the Fe spin state is different from that between the itinerary electrons and the molecular spin state, and/or (2) the Fe spin density is different from the molecular spin density [39,46,47]. The spatial distributions of the three Kondo resonance parameters (normalized amplitude, line-shape factor q, and Kondo temperature) are symmetric with respect to the two perpendicular molecular axes, corroborating the molecule's C_{2v} symmetry.

Figure 2(e) is a two-dimensional (2D) q map (constructed by acquiring point-by-point tunneling spectra in a 50×50 grid over the molecule), showing a minimum with a negative value at the molecule center, and two maxima with positive values at the two pyrrole rings along the main axis. Figure 2(f) is a 2D T_k map, showing higher T_k at the molecule center and lower T_k at the two pyrrole rings along the main axis. The 2D maps can be viewed as a superposition of two components. One component can be attributed to the Fe spin state which is located at the molecule center, contributes negative q and higher T_k (150–170 K). The other component can be attributed to the spin-polarized molecular state at 0.2 V [cf. Fig. 1(d)] which matches the Kondo resonance spatially [41]. This state is located at the two pyrrole rings, contributes positive q and lower T_k(120–130 K). In the following, we present the results of SP-DFT calculations to substantiate this assignment.

DFT optimized structures of FeTPP and H_2TPP adsorbed on the Au(111) substrate are shown in Figs. 3(a) and 3(h), respectively. In gas phase, both molecules have a planar macrocyclic ring with D_{4h} symmetry, whereas upon adsorption on Au(111), both molecules adopt a saddle-shaped conformation with C_{2v} symmetry [48]. The structural distortion can be clearly seen in the enlarged view of an adsorbed FeTPP [Fig. 3(b)] and a free one [Fig. 3(c)]. The macrocyclic ring of the free FeTPP is planar and the Fe rests at its center. In the adsorbed FeTPP, the two opposite pyrrole rings tilt upward [the arrows in the up panels in Figs. 3(a) and 3(h) point the up-titled pyrrole rings. The side views shown in the bottom panels follow the arrows' direction], while the other two pyrrole rings tilt downward. Additionally, the central Fe shifts slightly downward, resulting in a pyramidal coordination geometry in which the Fe-N bonds are 2.06 Å, being elongated as compared to 1.96 Å in the free molecule [6,11]. The Fe is 2.98 Å above the Au atom, within the range for weak Fe-Au binding. Bader charge analysis and $3d$ orbital occupation of the free and adsorbed FeTPP are shown in Table I. Note that the charge values are not absolute charges, but are still useful for comparison. The Fe in the free FeTPP is less positively

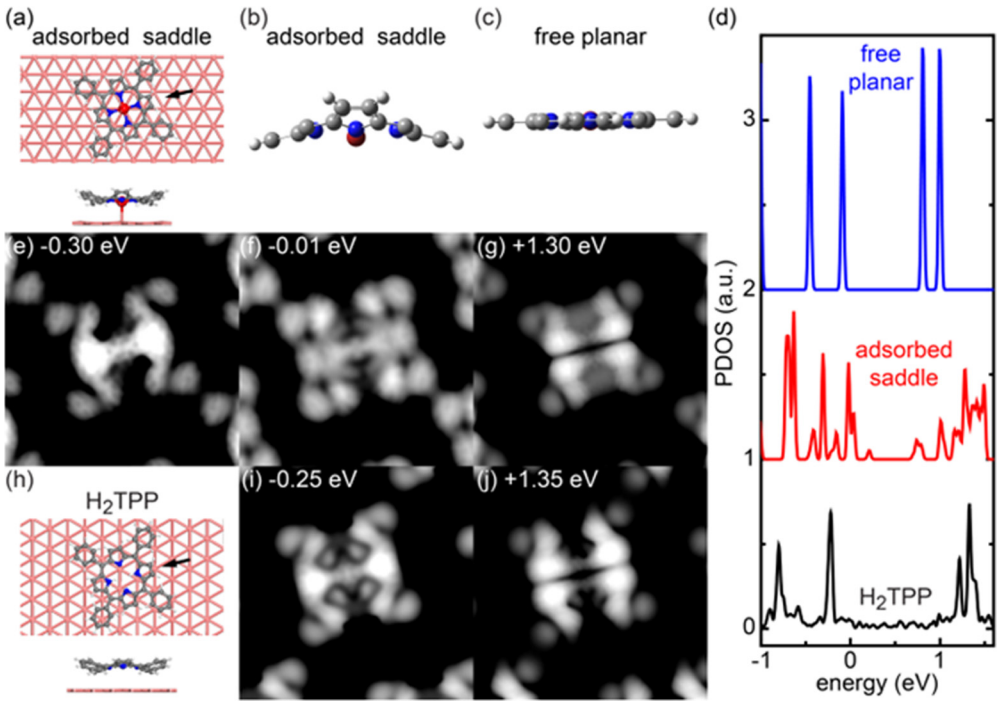

FIG. 3. (Color online) DFT optimized structure of FeTPP (a) and H_2TPP (h) adsorbed on a three-layer Au substrate (only the top layer is shown). (b), (c) Magnified side views of an adsorbed FeTPP and a free FeTPP showing the structural deformation of the macrocyclic ring upon adsorption. (d) PDOS of free FeTPP, adsorbed FeTPP and adsorbed H_2TPP (vertically shifted for clarity). (e)–(g) Constant PDOS contour maps of FeTPP at the indicated energy. (i), (j) Constant PDOS contour maps of H_2TPP at the indicated energy.

charged as compared to the adsorbed one ($+0.68\,e$ vs $+1.28\,e$) Nevertheless, $3d$ orbital occupations of the two species are similar, namely, 6.21 (6.07) for the adsorbed (free) FeTPP, evidencing that the Fe is of $3d^6$ in both configurations.

The calculated projection densities of states (PDOS) of H_2TPP [bottom curve in Fig. 3(d)] have two single peaks at -0.8 and -0.25 eV, and double peaks at 1.2/1.3 eV. The -0.25 eV peak corresponds to HOMO and the 1.2/1.3 eV peak LUMO. The PDOS of FeTPP [middle curve in Fig. 3(d)] has two major peaks at $-0.6/-0.7$ eV and -0.3 eV, a series of peaks around $\sim$1.3 eV, and double peaks at the Fermi level. Figure 3 also presents the equal density contours at the indicated energies (denoted as PDOS maps) of the two molecules. The constant PDOS contour map of FeTPP at -0.3 eV [Fig. 3(e)] exhibits a pattern resembling the H_2TPP HOMO [Fig. 3(i)], displaying two maxima distributed at the two up-tilted pyrrole rings and a dim dot at each of the four corners. Compared with the experimental STS images shown in Figs. 1(c) and 1(g), these maps capture the characteristic features of the -1.1-V state of the FeTPP and the -0.8-V state of the H_2TPP. The constant PDOS contour maps of FeTPP at 1.3 eV [Fig. 3(g)] and the H_2TPP LUMO [Fig. 3(j)] show four maxima separated by two nodal planes that run along and perpendicular to the main molecular axis, respectively. These features are comparable to the four-leaf clover pattern resolved in the 1.4-V state of the FeTPP [Fig. 1(e)] and the 1.6-V state of the H_2TPP [Fig. 1(h)]. We assign the -0.8 -V and 1.6 -V dI/dV peaks acquired at H_2TPP to HOMO and LUMO (note that DFT usually undermines the HOMO-LUMO gap), and the -1.1 -V and 1.4 -V dI/dV peaks acquired at FeTPP to the -0.3- and 1.3-eV states. The main axis defined in Figs. 1 and 2 passes through the two up-tilted pyrrole rings. The state at the Fermi level of FeTPP is associated with Fe because it is present in FeTPP but absent in H_2TPP. Interestingly, Fig. 3(f) shows that this state is not localized at Fe but extends over the macrocyclic ring, particularly, at the two up-titled pyrrole rings. The shape of this new state matches the H_2TPP HOMO, so we attribute this state to hybridization of the H_2TPP HOMO with a Fe $3d$ orbital (will discuss later). The 0.2 -V dI/dV peak of FeTPP is assigned to this hybridized state. Note that the PDOS map of this state [Fig. 3(f)] exhibits a mirror symmetry that is in accordance with the STS image of the 0.2-V state [Fig. 1(d)]. However, the fine features are not in good agreement. We attribute the discrepancy to tip convolution effects. To elucidate the effects of adsorption, the PDOS of a free FeTPP in gas phase is plotted in Fig. 3(d) above. Compared with the free molecule, adsorption does not change the major PDOS features, although broadening and satellite peaks can be seen, presumably due to molecular deformation and hybridization with the substrate states.

TABLE I. Bader charge analysis (units in e) and Fe $3d$ orbital occupation of FeTPP in four configurations. Positive values mean lose electrons.

FeTPP	Fe	TPP	Au sub.	Fe $3d$ Occup.
Free planar ($S=1$)	0.68	-0.68		6.07
Free saddle ($S=1$)	1.05	-1.05		6.19
Free saddle ($S=2$)	1.29	-1.29		6.02
Adsorbed saddle ($S=2$)	1.28	-0.86	-0.42	6.21

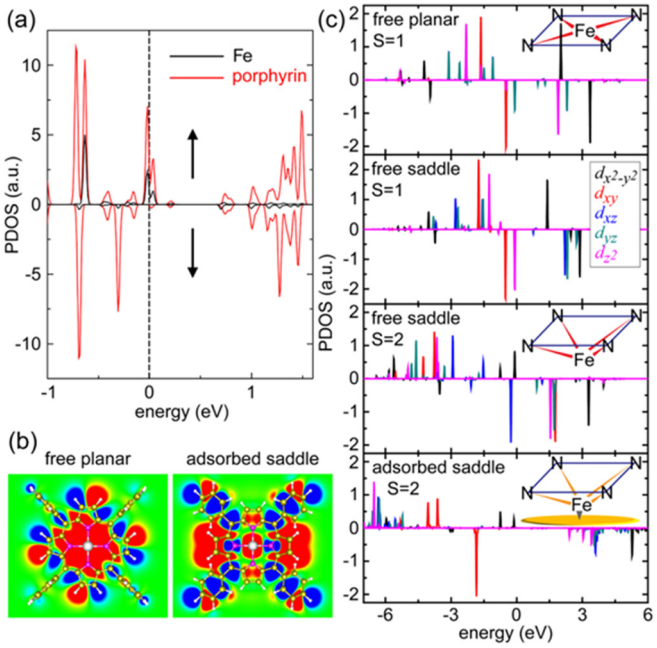

FIG. 4. (Color online) (a) Spin-polarized PDOS of Fe and porphyrin backbone of FeTPP adsorbed on an Au substrate. (b) Net spin density of free and adsorbed FeTPP (up spin and down spin are in red and blue, respectively). (c) Spin-polarized 3d orbitals of Fe in free, free saddle-shaped ($S = 1$ and 2) and adsorbed saddle-shaped molecules (from top to bottom).

The spin-polarized PDOS of the Fe and the TPP molecular backbone are plotted in Fig. 4(a). The Fe states are strongly polarized in this energy range [full PDOS can be found in Fig. 4(c)], with up spin being the major spin channel. As discussed before, the state near the Fermi level emerges upon Fe metalation. This state deserves detail inspections: First, Fig. 3(f) reveals that this state is not localized at Fe but extends over the two up-tilted pyrrole rings. Second, this state is strongly hybridized with the Fe state as the two occur at the same energy level. Third, this state is spin polarized and follows the same spin polarization as the Fe ion [15,49]. It is worthwhile to point that the -0.3-eV state is polarized antiparallel to the Fe majority spin. Both the -0.3-eV state [Fig. 3(e)] and the Fermi-level state [Fig. 3(f)] exhibit a shape comparable to the HOMO of the free-base H_2TPP [Fig. 3(i)]. We propose that Fe metalation splits the H_2TPP HOMO into two states: a fully occupied down-spin channel which is down-shifted to -0.3 eV and a partially occupied up-spin channel which is up-shifted to the Fermi level. As a result, the MO becomes a spin-polarized state. Herein, the Fe ion plays two roles: (1) it lifts the degeneracy of two spin channels of the HOMO, and (2) it spin polarizes the HOMO by pushing the up-spin channel to the Fermi level.

The net spin density map of the FeTPP adsorbed on Au(111) is plotted in the right panel of Fig. 4(b). In addition to the up-spin density at the central Fe, the porphyrin backbone also displays appreciable net spin density. In particular, a salient up-spin density (in red) can be found at the two pyrrole rings along the main axis. This picture concurs the intramolecularly resolved Kondo resonance presented in Fig. 2: the Kondo resonance amplitude profile [top panel of Fig. 2(d)] is in accord with the net spin density which peaks at the central Fe as well as at the two up-tilted pyrrole rings. The contrast resolved in the 2D T_k and q maps is very interesting. One explanation is that the 2D T_k and q maps reflect distinctive characteristics of the molecular spin states in contrast to the Fe spin states, for instance, different spatial orientations of the spin-polarized orbitals, different coupling strength with the screening electrons, etc. Nevertheless, it has been shown that hybridization effects may have an impact on T_k and q [43]. If the charge is inhomogeneously distributed in the molecule, the hybridization effects may contribute to a spatial variation of T_k and q too [28]. Our data are not conclusive for identifying which mechanism leads to the T_k and q contrast.

The net spin density map of the free FeTPP in gas phase is plotted in the left panel of Fig. 4(b), showing delocalized distribution of spin density over the central Fe and four pyrrole rings. The contrast between the two net spin density maps implies that adsorption on an Au surface significantly modifies FeTPP's spin state. In the following, we discuss how adsorption on an Au surface changes the spin state of the molecule. In Fig. 4(c), spin-polarized Fe 3d orbitals in the free FeTPP (top) and the adsorbed FeTPP (bottom) are plotted. Although in both cases Fe is of $3d^6$, the two molecules possess different spin configurations: Fe(II) is at $S = 1$ state with a magnetic moment of 2.1 μ_B in the free molecule, while Fe(II) is at $S = 2$ state with a magnetic moment of 3.7 μ_B in the adsorbed molecule. It is well established that in a free FeP molecule, the Fe ion is in a ligand field of D_{4h} point group [cf. inset in Fig. 4(c)] and has an empty d_{x2-y2} orbital and two degenerated d_{xz} and d_{yz} orbitals. Surface adsorption distorts the molecule macrocyclic ring and thus breaks the D_{4h} ligand field, which switches Fe(II) into a high-spin state. This phenomenon occurs in chemisorbed FeP on Co and Ni(001) as well as on Ni(110) and Ni(111) [9,10]. Generally speaking, elongated Fe-N bonds favor the high-spin state [50]. For example, strong covalent interaction of FeP with Co and Ni(001) substrate or FeP adsorbed at a divacancy site in a strained graphene lattice may increase Fe-N bond lengths and hence switches Fe(II) to a high-spin state [10,11]. As mentioned earlier, the Fe-N bonds of the FeTPP adsorbed on Au(111) are elongated to 2.06 Å, which concomitants with the spin switching.

In order to understand the roles of the Au surface in the spin switching, we studied a free-standing FeTPP with the same saddle-shaped conformation as the adsorbed one. Surprisingly, the calculations indicate that $S = 1$ and 2 states are nearly degenerate. In comparison, the $S = 2$ state is more stable (0.95 eV lower in total energy) for the adsorbed FeTPP. The saddle-shaped deformation and Fe-N bond elongation to 2.06 Å cannot fully account for the spin switching. The spin-polarized 3d orbitals of the two nearly degenerate states are plotted in the middle two panels of Fig. 4(c). Comparing the PDOS of the saddle-shaped molecule with and without the substrate [bottom two panels of Fig. 4(c)], one finds that the d orbitals are rearranged upon adsorption, indicating that the Fe ligand field is altered in the presence of the Au substrate. As shown in Table I, Fe (TPP backbone) is more positively (negatively) charged when the molecule changes its conformation from planar to saddle shape. After adsorption on Au, a partial

charge transfer of 0.42 electrons from the TPP backbone to the Au substrate occurs. As a consequence, Coulomb interaction between the TPP backbone and the Fe ion is weakened. We propose that, in addition to saddle-shaped deformation of the macrocyclic ring, there are two other mechanisms for stabilizing the high-spin state, as schematically illustrated in the inset in Fig. 4(c): weak chemical interaction between Fe ion and the underneath Au atom and charge transfer, by which the Fe-N bonds are weakened, thus the basal plane bonding towards the Fe weakened. Both mechanisms may additionally cause the Fe ligand field to deviate from D_{4h} to pyramidal geometry to favor the $S = 2$ spin state [11,50].

IV. CONCLUSIONS

In conclusion, we have probed the electronic and spin states of FeTPP adsorbed on Au(111) by resolving the intramolecular distribution of Kondo resonance. A comparison of the free-base H_2TPP and the FeTPP, which is rationalized by spin-polarized DFT calculations, reveals that HOMO of the former is spilt and spin polarized by Fe metalation. Furthermore, three adsorption-induced effects cooperatively transform the Fe ligand field from D_{4h} to pyramidal coordination geometry to drive the spin switching from an intermediate spin ($S = 1$) to a high spin ($S = 2$).

ACKNOWLEDGMENTS

This work was supported by Hong Kong RGC (Grant No. 603611) and National Science Foundation of China (Grants No. 11474145, No. 11334003, and No. 11104272). R.P. and X.S. also thank the National Supercomputing Center in Shenzhen for providing computation time.

[1] *Iron Porphyrins*, Part 3, edited by A. B. P. Lever and H. B. Gray (Wiley, New Jersey (1989).
[2] J. P. Collman, L. L. Hoard, N. Kim, G. Lang, and C. A. Reed, J. Am. Chem. Soc. **97**, 2676 (1975).
[3] M-S. Liao and S. Scheiner, J. Chem. Phys. **116**, 3635 (2002).
[4] M. E. Ali, B. Sanyal, and P. M. Oppeneer, J. Phys. Chem. B **116**, 5849 (2012).
[5] S. Bhandary, B. Brena, P. M. Panchmatia, I. Brumboiu, M. Bernien, C. Weis, B. Krumme, C. Etz, W. Kuch, H. Wende, O. Eriksson, and B. Sanyal, Phys. Rev. B **88**, 024401 (2013).
[6] M. G. Betti, P. Gargiani, C. Mariani, S. Turchini, N. Zema, S. Fortuna, A. Calzolari, and S. Fabris, J. Phys. Chem. C **116**, 8657 (2012).
[7] S. Stepanow, A. L. Rizzini, C. Krull, J. Kavich, J. C. Cezar, F. Yakhou-Harris, P. M. Sheverdyaeva, P. Moras, C. Carbone, G. Ceballos, A. Mugarza, and P. Gambardella, J. Am. Chem. Soc. **136**, 5451 (2014).
[8] Z. Hu, B. Li, A. Zhao, J. Yang, and J. G. Hou, J. Phys. Chem. C **112**, 13650 (2008).
[9] C. Wäckerlin, K. Tarafder, D. Siewert, J. Girovsky, T. Hählen, C. Iacovita, A. Kleibert, F. Nolting, T. A. Jung, P. M. Oppeneer, and N. Ballav, Chem. Sci. **3**, 3154 (2012).
[10] L. Liu, K. Yang, Y. Jiang, B. Song, W. Xiao, L. Li, H. Zhou, Y. Wang, S. Du, M. Ouyang, W. A. Hofer, A. H. C. Neto, and H.-J. Gao, Sci. Rep. **3**, 1210 (2013).
[11] S. Bhandary, S. Ghosh, H. Herper, H. Wende, O. Eriksson, and B. Sanyal, Phys. Rev. Lett. **107**, 257202 (2011).
[12] S. Bhandary, O. Eriksson, and B. Sanyal, Sci. Rep. **3**, 3405 (2013).
[13] J. Brede, N. Atodiresei, S. Kuck, P. Lazić, V. Caciuc, Y. Morikawa, G. Hoffmann, S. Blügel, and R. Wiesendanger, Phys. Rev. Lett. **105**, 047204 (2010).
[14] N. Atodiresei, J. Brede, P. Lazić, V. Caciuc, G. Hoffmann, R. Wiesendanger, and S. Blügel, Phys. Rev. Lett. **105**, 066601 (2010).
[15] H. Wende, M. Bernien, J. Luo, C. Sorg, N. Ponpandian, J. Kurde, J. Miguel, M. Piantek, X. Xu, Ph. Eckhold, W. Kuch, K. Baberschke, P. M. Panchmatia, B. Sanyal, P. M. Oppeneer, and O. Eriksson, Nat. Mater. **6**, 516 (2007).
[16] M. Bernien, J. Miguel, C. Weis, M. E. Ali, J. Kurde, B. Krumme, P. M. Panchmatia, B. Sanyal, M. Piantek, P. Srivastava, K. Baberschke, P. M. Oppeneer, O. Eriksson, W. Kuch, and H. Wende, Phys. Rev. Lett. **102**, 047202 (2009).
[17] H. C. Herper, M. Bernien, S. Bhandary, C. F. Hermanns, A. Krüger, J. Miguel, C. Weis, C. Schmitz-Antoniak, B. Krumme, D. Bovenschen, C. Tieg, B. Sanyal, E. Weschke, C. Czekelius, W. Kuch, H. Wende, and O. Eriksson, Phys. Rev. B **87**, 174425 (2013).
[18] M. Bernien, X. Xu, J. Miguel, M. Piantek, Ph. Eckhold, J. Luo, J. Kurde, W. Kuch, K. Baberschke, H. Wende, and P. Srivastava, Phys. Rev. B **76**, 214406 (2007).
[19] M. D. Kuz'min, R. Hayn, and V. Oison, Phys. Rev. B **79**, 024413 (2009).
[20] P. Gargiani, G. Rossi, R. Biagi, V. Corradini, M. Pedio, S. Fortuna, A. Calzolari, S. Fabris, J. C. Cezar, N. B. Brookes, and M. G. Betti, Phys. Rev. B **87**, 165407 (2013).
[21] L. Gao, W. Ji, Y. B. Hu, Z. H. Cheng, Z. T. Deng, Q. Liu, N. Jiang, X. Lin, W. Guo, S. X. Du, W. A. Hofer, X. C. Xie, and H.-J. Gao, Phys. Rev. Lett. **99**, 106402 (2007).
[22] A. Mugarza, R. Robles, S. Stepanow, G. Ceballos, and P. Gambardella, Nat. Commun. **2**, 490 (2011).
[23] N. Tsukahara, S. Shiraki, S. Itou, N. Ohta, N. Takagi, and M. Kawai, Phys. Rev. Lett. **106**, 187201 (2011).
[24] E. Minamitani, N. Tsukahara, D. Matsunaka, Y. Kim, N. Takagi, and M. Kawai, Phys. Rev. Lett. **109**, 086602 (2012).
[25] B. W. Heinrich, G. Ahmadi, V. L. Müller, L. Braun, J. I. Pascual, and K. J. Franke, Nano Lett. **13**, 4840 (2013).
[26] J. P. Perdew, K. Burke, and M. Ernzerhof, Phys. Rev. Lett. **77**, 3865 (1996).
[27] J. Klimeš, D. R. Bowler, and A. Michaelides, Phys. Rev. B **83**, 195131 (2011).
[28] U. G. E. Perera, H. J. Kulik, V. Iancu, L. G. G. V. D. da Silva, S. E. Ulloa, N. Marzari, and S. W. Hla, Phys. Rev. Lett. **105**, 106601 (2010).
[29] S. L. Dudarev, G. A. Botton, S. Y. Savrasov, C. J. Humphreys, and A. P. Sutton, Phys. Rev. B **57**, 1505 (1998).
[30] M. Cococcioni and S. de Gironcoli, Phys. Rev. B **71**, 035105 (2005).

[31] L. Wei, Y. She, Y. Yu, X. Yao, and S. Zhang, J. Mol. Model. **18**, 2483 (2012).
[32] Y. Zhang and H. Jiang, J. Chem. Theor. Comput. **7**, 2795 (2011).
[33] G. Kresse and J. Furthmuller, Phys. Rev. B **54**, 11169 (1996).
[34] G. Kresse and D. Joubert, Phys. Rev. B **59**, 1758 (1999).
[35] P. Giannozzi, S. Baroni, N. Bonini, M. Calandra, R. Car, C. Cavazzoni, D. Ceresoli, G. L. Chiarotti, M. Cococcioni, I. Dabo, A. Dal Corso, S. de Gironcoli, S. Fabris, G. Fratesi, R. Gebauer, U. Gerstmann, C. Gougoussis, A. Kokalj, M. Lazzeri, L. Martin-Samos, N. Marzari, F. Mauri, R. Mazzarello, S. Paolini, A. Pasquarello, L. Paulatto, C. Sbraccia, S. Scandolo, G. Sclauzero, A. P. Seitsonen, A. Smogunov, P. Umari, and R. M. Wentzcovitch, J. Phys.: Condens. Matter **21**, 395502 (2009).
[36] W. Auwärter, A. Weber-Bargioni, S. Brink, A. Riemann, A. Schiffrin, M. Ruben, and J. V. Barth, Chem. Phys. Chem. **8**, 250 (2007).
[37] F. Buchner, V. Schwald, K. Comanici, H.-P. Steinrück, and H. Marbach, Chem. Phys. Chem. **8**, 241 (2007).
[38] L.A. Zotti, G. Teobaldi, W.A. Hofer, W. Auwarter, A. Weber-Bargioni, and J.V. Barth, Surf. Sci. **601**, 2409 (2007).
[39] V. Iancu, A. Deshpande, and S.-W. Hla, Phys. Rev. Lett. **97**, 266603 (2006).
[40] U. Fano, Phys. Rev. **124**, 1866 (1961).
[41] A. Mugarza, R. Robles, C. Krull, R. Korytár, N. Lorente, and P. Gambardella, Phys. Rev. B **85**, 155437 (2012).
[42] H. Prüser, M. Wenderoth, A. Weismann, and R. G. Ulbrich, Phys. Rev. Lett. **108**, 166604 (2012).
[43] N. Néel, J. Kröger, R. Berndt, T. O. Wehling, A. I. Lichtenstein, and M. I. Katsnelson, Phys. Rev. Lett. **101**, 266803 (2008).
[44] V. Madhavan, W. Chen, T. Jamneala, M. F. Crommie, and N. S. Wingreen, Science **280**, 567 (1998).
[45] O. Ujsaghy, J. Kroha, L. Szunyogh, and A. Zawadowski, Phys. Rev. Lett. **85**, 2557 (2000).
[46] Q. Li, S. Yamazaki, T. Eguchi, H. Kim, S.-J. Kahng, J. F. Jia, Q. K. Xue, and Y. Hasegawa, Phys. Rev. B **80**, 115431 (2009).
[47] N. Knorr, M. A. Schneider, L. Diekhöner, P. Wahl, and K. Kern, Phys. Rev. Lett. **88**, 096804 (2002).
[48] A. Weber-Bargioni, W. Auwärter, F. Klappenberger, J. Reichert, S. Lefrançois, T. Strunskus, Ch. Wöll, A. Schiffrin, Y. Pennec, and J. V. Barth, Chem. Phys. Chem. **9**, 89 (2008).
[49] F. Djeghloul, F. Ibrahim, M. Cantoni, M. Bowen, L. Joly, S. Boukari, P. Ohresser, F. Bertran, P. Le Fèvre, P. Thakur, F. Scheurer, T. Miyamachi, R. Mattana, P. Seneor, A. Jaafar, C. Rinaldi, S. Javaid, J. Arabski, J. P. Kappler, W. Wulfhekel, N. B. Brookes, R. Bertacco, A. Taleb-Ibrahimi, M. Alouani, E. Beaurepaire, and W. Weber, Sci. Rep. **3**, 1272 (2013.)
[50] W. R. Scheidt and C. A. Reed, Chem. Rev. **81**, 543 (1981).